ELSEVIER

Journal of Chromatography A, 877 (2000) 109–122

JOURNAL OF CHROMATOGRAPHY A

www.elsevier.com/locate/chroma

Adsorption behavior and prediction of the band profiles of the enantiomers of 3-chloro-1-phenyl-1-propanol Influence of the mass transfer kinetics

Djamel E. Cherrak[a,b], Saad Khattabi[a,c], Georges Guiochon[a,b,*]

[a]*Department of Chemistry, University of Tennessee, Knoxville, TN 37996-1600, USA*

[b]*Division of Chemical and Analytical Sciences, Oak Ridge National Laboratory, Knoxville, TN 37831-6120, USA*

[c]*Department of Food Science and Technology, University of Tennessee, Knoxville, TN 37996-1071, USA*

Received 28 March 1999; received in revised form 20 December 1999; accepted 7 February 2000

Abstract

The single-component and competitive adsorption isotherms of the enantiomers of 3-chloro-1-phenyl-1-propanol were measured by frontal analysis. The stationary phase was a cellulose tribenzoate coated on silica, the mobile phase an *n*-hexane–ethyl acetate (95:5) solution. The adsorption data measured fitted well to the Langmuir isotherm model. The band profiles of single components and of their mixtures were calculated using the equilibrium-dispersive model. These profiles were found to match quite satisfactorily the experimental band profiles. However, the agreement between calculated and experimental band profiles was significantly improved when a more complex model taking into account the mass transfer kinetics was used. The mass transfer rate coefficients, k_f, for both single components were determined by using the transport-dispersive model of chromatography. The coefficients obtained were used to predict the band profiles of mixtures of the two enantiomers to good agreement.

Keywords: Adsorption isotherms; Mass transfer; Enantiomer separation; Chiral stationary phases, LC; Band profiles; 3-Chloro-1-phenyl-1-propanol

1. Introduction

Enantiomeric separations is a topic of great current interest in liquid chromatography because of its importance for the pharmaceutical industry, most compounds used as drugs being chiral. Preparative chromatography is becoming widely used for the purification of enantiomers of synthesis intermediates, at least at the drug development stage, mostly because of the low cost of this method compared to that of the more conventional approach of designing a stereoselective organic synthesis. However, this procedure needs to be optimized in order to achieve the minimum production cost and the desired purity of the enantiomers. Optimization of a separation is particularly critical when operating a simulated moving bed unit in which case the selection of the operation parameters cannot be done effectively by the time-honored method of trial-and-error but requires a more sophisticated approach [1–6]. The reason for this is in the number of the parameters involved and in the intricacy of their

*Corresponding author. Tel.: +1-865-974-0733; fax: +1-865-974-2667.

E-mail address: guiochon@utk.edu (G. Guiochon)

0021-9673/00/$ – see front matter
PII: S0021-9673(00)00189-8

interactions with the product purity and throughput, especially under nonlinear conditions. Among these parameters, the most important are those of the equilibrium isotherms of the enantiomers to be separated [7]. Modeling the preparative separation of a pair of enantiomers and studying the dependence of the results on the system parameters is probably the safest and cheapest method of optimizing their production. This requires, however, the prior determination of accurate equilibrium data and their modeling.

Most chiral stationary phases (CSP) commercially available are made by bonding to a silica surface the pure enantiomer of a small chiral molecule [8] or macromolecule (e.g. a protein or a derivatized cellulose) [5,8–10]. The mechanism of enantioseparations is still not completely understood, in large part because of the paucity of the results available. Paradoxically, although they do not give the best analytical separations and give poor performance in preparative applications, the behavior of silica-bonded proteins [9–11] is better understood than that of silica-coated celluloses [5,6,8,12,13]. This is probably related to the easy identification of well-defined chiral sites in proteins while the structure of cellulose is most complex. However, cellulose-based stationary phases are most suitable for preparative enantioseparations [12], due to their high loadability and their good mechanical stability. Thus, it seems useful to undergo a systematic investigation of the equilibrium isotherms of pairs of enantiomers on different such phases.

Previous studies showed that the adsorption data of many enantiomers on several chiral stationary phase could be accounted for by the bi-Langmuir isotherm model [4,10–15]. However, other studies suggested different models, e.g. the sum of a linear term and a Langmuir isotherm [4] or more complex models [12,15]. The bi-Langmuir model assumes the surface of the stationary phase to be heterogeneous and covered with two types of adsorption sites [7,10,14,15]. The more abundant type of sites are low-energy, nonselective sites, characterized by a fast mass transfer kinetics. They significantly contribute to the retention but have no role in the enantioseparation. The second type of site is associated with the bonded ligands and is responsible for chiral recognition. These are high energy sites, characterized by a slow mass transfer kinetic which may cause an important band broadening in some cases [7,15]. Although this model accounts well for the data acquired on bonded proteins [7,9–11,14,15], its validity for enantiomeric adsorption on cellulose-based phases is questionable [12,13]. Systematic investigations of the adsorption behavior of pairs of enantiomers on this important type of stationary phase, which is most useful in preparative chromatography, would lead to a better understanding of the physico-chemical features underlying the retention and separation of enantiomers.

In this study, we measured the single-component and the competitive isotherm adsorption data of the enantiomers of 3-chloro-1-phenyl-1-propanol on cellulose tribenzoate. We show how these data are measured and modeled and compare the experimental band profiles of large samples with those calculated. The predictions given by the equilibrium-dispersive and the transport-dispersive models of chromatography were compared. The influence of the mass transfer kinetics on the elution bands was also studied.

2. Experimental

2.1. Equipment

All experiments were carried out with a HP 1090 liquid chromatograph (Hewlett-Packard, Palo Alto, CA, USA), equipped with a ternary-solvent delivery system, an automatic sample injector with a 250-μl loop, a diode-array UV detector, and a computer data acquisition system using the HP-Chem Station software (Ver. A.05.03). Acquired data were downloaded to one of the computers of the University of Tennessee Computer Center for further data processing.

2.2. Column

A 25×0.46 cm I.D. Chiracel OB-H (cellulose tribenzoate coated on silica gel substrate) column (Daicel, Tokyo, Japan), packed with 5-μm particles, was used. The total porosity (ε_T=0.77) was determined by injecting 1,3,5-tri-*tert.*-butyl benzene on the column. This compound is not retained on

Chiracel OB-H under the actual experimental conditions [13,16–18].

2.3. Mobile phase and chemicals

HPLC-grade *n*-hexane and ethyl acetate were purchased from Fisher Scientific (Fair Lawn, NJ, USA). *S*- and *R*-3-chloro-1-phenyl-1-propanol (CPP) (purity>99%) and 1,3,5-tri-*tert*.-butyl benzene (TTBB) were purchased from Aldrich (Milwaukee, WI, USA). These products were used without further purification.

2.4. Procedures

All experiments were performed with a mixture of *n*-hexane–ethyl acetate (95:5 v/v) as the mobile phase, at room temperature, and with a flow-rate of 1 ml min^{-1}.

2.5. Characteristics of the analytical chromatograms

The retention factors of both enantiomers and the efficiencies of their peaks are reported in Table 1. Although, the selectivity factor was small ($\alpha = 1.20$), a complete separation between *S*- and *R*-CPP was achieved at infinite dilution (see chromatograms later). This result is explained by the high column efficiency, about 8000 theoretical plates. This efficiency was determined from the width of the peak at half-height and its retention time. It was measured with small low-concentration samples under conditions such that bC_M is smaller than 0.01, where b is the coefficient of the Langmuir isotherm (see later) and C_M is the maximum solute concentration in the eluted peak.

Table 1
Experimental data of CPP enantiomers under linear conditions[a]

Enantiomer	*S*	*R*
Retention time (min)	9.04	10.27
k	1.83	2.21
Number of plates[b]	8200	8000

[a] $t_0 = 3.2$ min determined by injecting TTBB (non-retained component).

[b] The column efficiency is determined from the width at the half-height of the peak maximum; selectivity factor (α) = 1.21.

2.6. Determination of the adsorption isotherm for single component

The single-component and competitive adsorption isotherms of the two CPP enantiomers were measured using frontal analysis in the single-step mode [4]. Two containers of the solvent delivery system were filled, one with pure mobile phase and the other with a solution of the CPP enantiomers at the desired concentrations. Suitable programming of the controller of the solvent delivery system made it easy to perform the required series of 10 concentration steps, i.e. of injections of 10 wide (ca. 4 min) rectangular injections with a maximum concentration increasing from $0.1C_0$ to C_0 in $0.1C_0$ steps. In all these experiments, the column was equilibrated with the pure mobile phase by percolating it with three column volumes of this solution after the elution of the sample and before the injection of a new sample. Despite this procedure being tedious, time consuming, and somewhat wasteful of chemicals, it has the advantage over the conventional staircase mode of avoiding the cumulative errors encountered in the calculation of the isotherm data points. Through the use of several enantiomer solutions of increasing concentrations, the total range of concentrations studied extended up to 5 g l^{-1}. The UV detector was calibrated at 270 nm, the absorbance data being transformed into concentrations by averaging the measurements made on each concentration plateau. The slightly nonlinear calibration curve was fitted to a second-order polynomial. Due to the achiral nature of the UV response, the same calibration curve was used for both enantiomers.

The amount of compound adsorbed by the stationary phase was determined from the inflection point of the breakthrough curve using the classical equation:

$$q = \frac{C(V_F - V_0)}{V_a} \quad (1)$$

where q is the amount adsorbed on the solid phase in equilibrium with the concentration C in the mobile phase, V_F is the retention volume of the inflection point of the breakthrough curve, V_0 is the column void volume, and V_a is the volume of adsorbent in the column. The use of the retention volume of the

inflection point is legitimate because the column efficiency was high (see earlier) [19]. FACP was also used to analyzed the rear diffuse boundary of the rectangular pulses, which provided further isotherm data.

2.7. Determination of the competitive adsorption isotherms

The competitive adsorption isotherms were measured using the method of single-step binary frontal analysis [7,20]. The same procedure was used as for the determination of single-component isotherms, except that the second container of the solvent delivery system was now filled with a solution of both enantiomers in the desired ratio. The advantage of this method over step frontal analysis is that the analysis of the relative concentrations of the two enantiomers in the eluate on the intermediate plateau is not needed since this plateau contains only the less retained *S*-enantiomer. The concentration of this compound at the intermediate plateau was calculated from the calibration curve at 270 nm. The adsorbed amount of each enantiomer in the mixture, q_x, was determined from the retention volumes and the corresponding concentrations, C_x, of the breakthrough curves using the equation given by Jacobson et al. [20]:

$$q_x = \frac{C_x(V_{S+R} - V_0) - C_{x,ip}(V_{S+R} - V_S)}{V_a} \quad (2)$$

where V_0, V_S, V_{S+R} and V_a are the column dead volume, the elution volumes of the two breakthrough fronts, and the volume of adsorbent in the column, respectively. $C_{x,ip}$ is the concentration of *S* enantiomer at the intermediate plateau.

2.8. Fitting of isotherm data to isotherm model

The experimental adsorption data were fitted to the Langmuir and the bi-Langmuir isotherm models. The equation of the competitive bi-Langmuir isotherm is:

$$q_i = \frac{a_{n,i}C_i}{1 + b_{n,1}C_1 + b_{n,2}C_2} + \frac{a_{s,i}C_i}{1 + b_{s,1}C_1 + b_{s,2}C_2} \quad (3)$$

In this equation, i corresponds to one of the two enantiomers; the a_j and b_j are numerical coefficients. It is common but not general in enantiomeric separations that the two terms of Eq. (3) correspond to the contributions of the nonselective and the selective interactions to the phase equilibrium isotherm, respectively [7,10,14]. Then, there are six coefficients since, obviously $a_{n,1} = a_{n,2}$ and $b_{n,1} = b_{n,2}$. All six coefficients may be different from zero but some may not. Although there are probably always nonselective interactions involved in the retention of enantiomers, their contribution may be negligibly small compared to that of the selective interactions, in which case a least-square fit of the experimental data to Eq. (3) fails to converge properly and the use of a Langmuir isotherm with $a_{n,i} = 0$ is required. There are obviously also cases in which a Langmuir or bi-Langmuir model does not allow a proper fit of the data. Then, more complex models must be considered. There was no such need in this study (see later).

The coefficients of the equilibrium isotherm model were calculated using a nonlinear regression program (Sigma Plot 4.00, SPSS, San Rafael, CA, USA). The best coefficients for the isotherm parameters were obtained by minimizing the following function:

$$\sigma^2 = \sum_{i=1}^{N_d} \frac{(q_i^{exp} - q_i^{th})^2}{(q_i^{exp})^2} \quad (4)$$

where N_d, q_i^{exp} and q_i^{th} are the number of data points, the experimental and the calculated value for each data points, respectively. Eq. (4) means that, in the regression, the experimental data were given a weight equal to the reverse of the stationary phase concentration.

2.9. Equilibrium-dispersive model

The band profiles were first calculated using the equilibrium-dispersive model of chromatography [7]. This model assumes an instantaneous equilibrium between the stationary and the mobile phase but accounts for the axial dispersion of the solute. However, the contribution of the mass transfer resistances can be included in the value of the axial dispersion coefficient (which becomes an apparent dispersion coefficient). Realistic band profiles are obtained [7] when this coefficient is related to the

column efficiency using the conventional equation of linear chromatography:

$$D_a = \frac{u_0}{2}\frac{L}{N} \quad (5)$$

where u_0 is the mobile phase linear velocity, L is the column length and N the number of theoretical plates. The reason for the general validity of the equilibrium-dispersive model is the high efficiency of the columns used in HPLC, even in industrial preparative applications. At high column efficiency, the propagation of the band profile is much more influenced by the nonlinear behavior of the equilibrium isotherm than by the mass transfer kinetics. It is not uncommon, however, that in enantioseparations the mass transfer kinetics is relatively slow, especially for the more retained enantiomer. Then a more complex model must be used for the calculation of band profiles.

2.10. Lumped kinetic model (transport-dispersive model)

In this study, we found (see later) that the solid film linear driving force model should be used to account for the mass transfer kinetics. This model assumes that the rate of variation of the stationary phase concentration is proportional to the difference between the equilibrium concentration of the solute in the stationary phase, q^* (when the mobile phase concentration is C) and the actual concentration. This leads to the following kinetic equation:

$$\frac{\partial q}{\partial t} = k_f(q^* - q) \quad (6)$$

where k_f is the mass transfer rate coefficient, proportional to the inverse of the average residence time. A combination of the same mass balance equation as used in the equilibrium-dispersive model but with the actual axial dispersion coefficient, and of Eqs. (3) and (5) can be solved numerically using the backward–forward finite difference method [7]. Still, the initial and boundary conditions must be defined.

2.11. Initial and boundary conditions

The initial condition characterizes the state of the column when the injection is performed. In this case, the column contained only the stationary phase in equilibrium with the pure mobile phase, free of sample:

$$C(t = 0, z) = 0 \quad (7)$$

The classical boundary conditions of nonlinear elution chromatography [7] were used, assuming a rectangular injection pulse with a width t_p and a maximum concentration C_0 at the column inlet.

$$\begin{aligned} &C(t = 0, z) = C_0, \ 0 \le t \le t_p \\ &C(t = 0, z) = 0, \ t < 0 \text{ or } t > t_p \end{aligned} \quad (8)$$

2.12. Determination of the experimental band profiles

Sufficiently large samples of solutions in the mobile phase of either the single components or binary mixtures of the enantiomers were injected in the column. To minimize the band dispersion caused by axial dispersion in the sampling device, upstream of the column, the sample solution was placed in one of the containers of the pumping system. A single-step positive concentration gradient followed by a negative one after an appropriate delay was performed to make each injection. The band was assumed to be a rectangular pulse. This assumption was supported by the steep boundaries of the records of the elution of samples from a zero-dead volume connector replacing the column (not shown).

3. Results and discussion

3.1. Modeling of equilibrium isotherms

The Scatchard plot (q/C vs. q) for the single-component data is shown in Fig. 1. The symbols represent the data points. The solid lines correspond to the best Langmuir isotherm (see later). The experimental data are well accounted for by the straight lines. This demonstrates that a Langmuir isotherm model accounts properly for the isotherm data of the two CPP enantiomers. This is not always the case in enantiomeric equilibria on cellulose-based packing materials [7,14]. For example, Charton et al. [13] have shown that the Langmuir model was not suitable in accounting for the adsorption behavior of

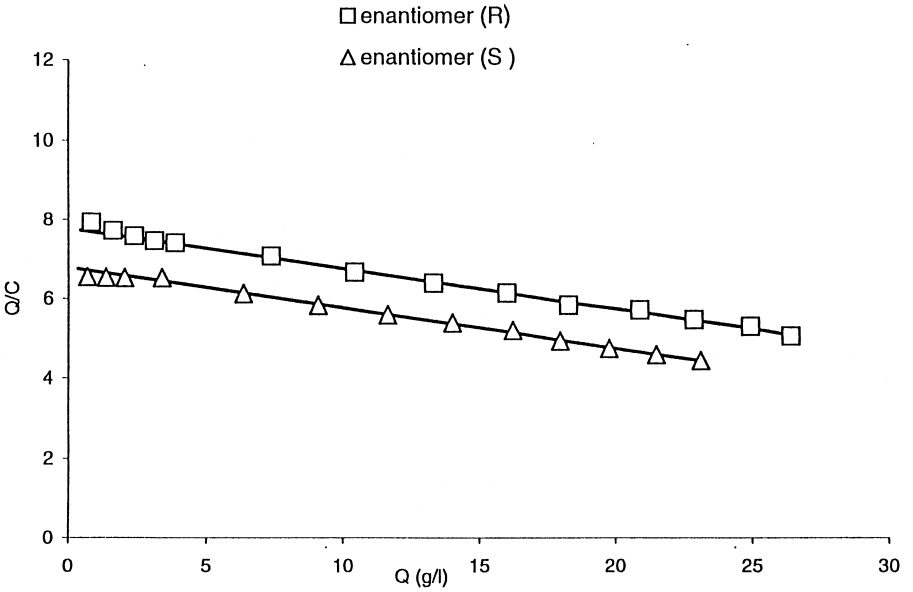

Fig. 1. Scatchard plots for the adsorption of the enantiomers of 3-chloro-1-phenyl-1-propanol on Chiracel OB-H measured by frontal analysis; mobile phase: hexane–ethyl acetate (95:5); flow-rate: 1 ml min^{-1}. Symbols: experimental data. Solid lines: calculated isotherms derived from the Langmuir isotherm model (see later).

the methyl mandelate enantiomers on 4-methylcellulose tribenzoate immobilized on silica, a stationary phase only slightly different from the one used in this work (cellulose tribenzoate coated on silica). In their study, the equilibrium isotherms were determined by frontal elution by characteristic point (FECP) and accounted for by a bi-Langmuir isotherm model [Eq. (2)]. Their model assumed that the stationary phase is heterogenous, that there is a mixed retention mechanism with two different types of interactions: (a) nonselective interactions characterized by a low interaction energy and a high saturation capacity; and (b) enantioselective interactions, characterized by a high interaction energy (narrow and nearly monodisperse) and a low saturation capacity ($q_{\text{enantioselective}} \ll q_{\text{nonselective}}$). The first type of interactions (i.e. the nonselective ones) contribute significantly to retention mainly if their large number makes their contribution significant in spite of their weak energy.

Fig. 2 shows the isotherm data (symbols) of *S*- and *R*-CPP determined by frontal analysis and FACP. The latter data were determined by integration of the rear diffuse boundary of the elution profile of a large sample (ca. 4 ml) of a concentrated solution of each pure enantiomer (ca. 5 g l^{-1}). For both enantiomers, these data points are slightly higher than those given by frontal analysis. This difference is more pronounced for *S*-CPP, the less retained enantiomer, especially at concentrations higher than 1 g l^{-1}. This effect can be attributed to a slow mass transfer kinetics which also causes a marked peak tailing, probably aggravated by a concentration-dependent rate-coefficient [7,15,21]. In principle, the column efficiency (see earlier, $N=8000$ plates) is high enough to allow the derivation of accurate isotherm data, even though the elution using the characteristic point (ECP or FACP) method is based on the ideal model (infinite column efficiency) [7]. However, because of the relatively slow mass transfer kinetics, the peak tails more than expected for the high value of the efficiency and the adsorption isotherm data derived by FACP are overestimated and less accurate. For the sake of comparison, the solid lines represent the best isotherm (see later).

The FA experimental isotherm data are reported in Fig. 2 (single-component data) and Fig. 3 (competitive isotherm data) and are shown as symbols. The entire set of data was used in the nonlinear regression which fitted all these data to Eq. (3). The solid

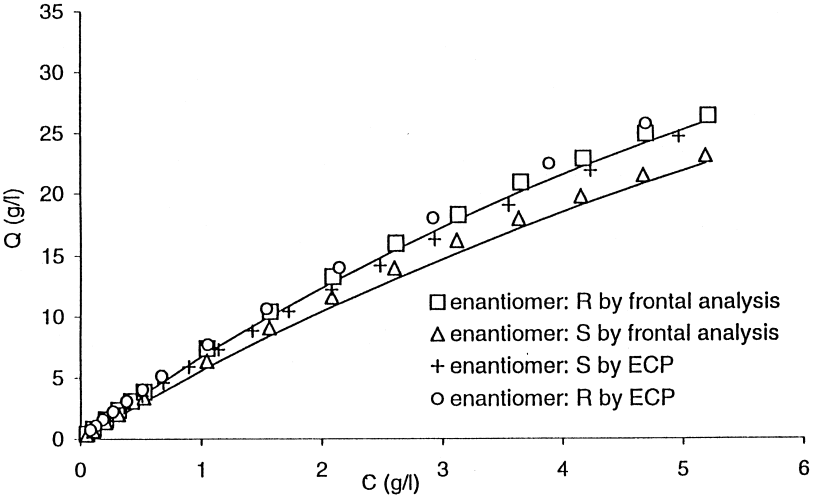

Fig. 2. Adsorption data for the enantiomers of 3-chloro-1-phenyl-1-propanol determined by frontal analysis and ECP (elution by characteristic points). Symbols: data points; solid lines: calculated isotherms derived from the competitive Langmuir model (see later).

lines in the figures show the best Langmuir isotherms calculated from the set of the best coefficients afforded by the regression (see below the reasons for the choice of $a_{n,i} = 0$ in this equation). There is a very good agreement between the whole set of experimental data and the result of the regression. Fig. 3 shows the competitive equilibrium isotherm data and the calculated isotherms for the two enantiomers at three different relative concentrations, for the racemic mixture (1:1) and for two enriched mixtures with relative compositions 1/3 and 3/1.

Table 2 illustrates the results of the different regressions performed and gives the values of the best parameters derived from these different isotherm

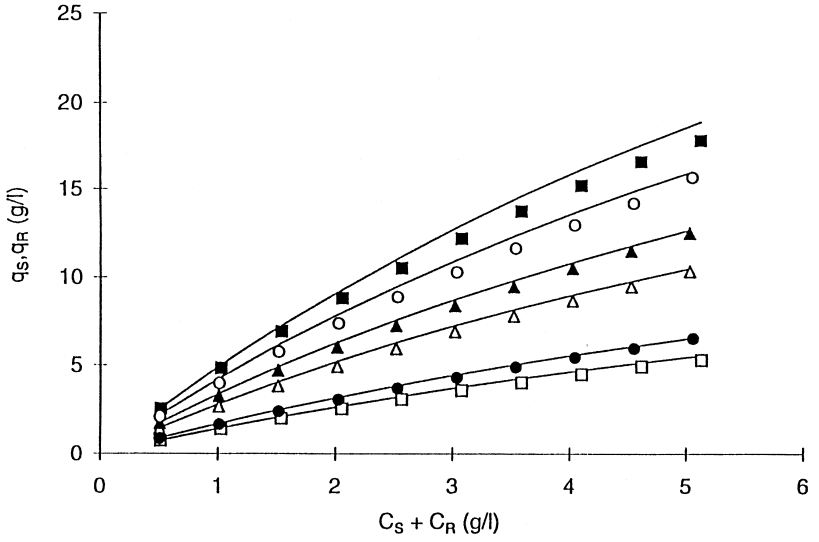

Fig. 3. Experimental competitive adsorption data for the *R* (solid symbols) and the *S* (open symbols) enantiomers and best calculated isotherms using the Langmuir competitive isotherm model (lines) for different mixtures. Ratios C_R/C_S: 3/1 (□); 1/1 (▽); 1/3 (○).

Table 2
Isotherm parameters of the two enantiomers obtained by regression (see Eq. (3))

Parameters	Site	Enantiomer	$a = q_s b$	b (l g^{-1})	SE, b[a]	RSD (%)	q_s (g l^{-1})	SE, q[a]	RSD (%)	PRESS
6	*n*-selective	*S*	2.55	0.087	0.149	170.7	29.24	132.19	452.1	97.2
		R								
	Selective	*S*	3.34	0.042	0.168	398.3	79.37	134.34	169.3	
		R	4.72	0.112	0.120	107.3	42.15	125.76	298.4	
5	*n*-selective	*S*	3.18	0.018	0.059	335.4	181.59	472.18	260.0	44.3
		R								
	Selective	*S*	2.82	0.156	0.029	18.3	18.05	16.01	88.7	
		R	4.76	0.264	0.116	43.9	18.05	16.01	88.7	
S Langmuir *R* bi-Langmuir	*n*-selective	*S*	5.34	0.042	0.010	24.8	127.38	28.65	22.5	1042.0
		R								
	Selective	*S*	0.00	–	–	–	–	–	–	
		R	1.38	0.196	0.130	66.2	7.07	0.20	10.7	
Langmuir		*S*	6.04	0.077	0.008	10.8	78.90	78.90	7.2	656.9
		R	7.24	0.091	0.008	9.2	79.29	79.29	5.9	

[a] SE, standard error.

models. These results are somewhat unusual and illustrate several situations commonly encountered in similar studies on phase equilibria. Two types of error figures are reported in this table. The PRESS number is the sum of the residuals or sum of the square of the differences between experimental and calculated values of q. It can be used as a gauge of how well a regression model predicts new data. In other words, the predictive ability of the model is better when the PRESS is smaller. The trend seen in the last column of Table 2 illustrates the well-known fact that increasing the number of parameters allows a better fit of the data. However, the relative standard deviation of the estimate of each parameter must also be taken into account when choosing the model that best fits the isotherm data.

The five-parameters bi-Langmuir model has the lowest PRESS number. However, it is characterized by enormous uncertainties in the values of the parameters. This arises from the numerical difficulty encountered in attempting to fit a set of experimental data on an equation such as Eq. (3). The calculation problem is indeterminate unless the saturation capacities of the two Langmuir terms differ by well above one order of magnitude (which was the case in studies cited earlier [7,13,14,15]). Obviously, the attempt can be fruitful only if the experimental data were also acquired in a wide range of concentrations [10,11]. Reducing the number of parameters from six [Eq. (3) for two enantiomers] to five (by further assuming that the two selective sites have the same saturation capacity [14], then that the first eluted enantiomer does not 'see' the selective sites [15]) does not improve the results. In the first case, the errors on the best estimates of the coefficients remain considerable. In the second case, the errors are still important and the PRESS number becomes very large.

This leaves as the best isotherm model the classical Langmuir model, with a set of four parameters, two different ones for each of the two enantiomers. Although the PRESS number is high compared to those obtained with the more complex bi-Langmuir model, this is compensated for and explained by the simplification resulting from a smaller number of parameters. Furthermore, there is a considerable improvement in the precision on each of the parameters (Table 2). Finally, the value of the separation factor, the ratio of the initial slopes of the isotherms of the two enantiomers (i.e. the ratio of the two a coefficients or of the sums of the a coefficients), is closer to the experimental value in this last case. Note that the saturation capacities of the two enantiomers are very close. Given the precision of the

measurements, they can be considered as identical which makes the competitive Langmuir model thermodynamically consistent in this case. The band profiles calculated from the competitive Langmuir model without corrections should account well for the experimental profiles.

3.2. Single-component band profiles

Fig. 4(a)–(d) show the band profiles obtained for four consecutive injections of increasing volumes of an *S*-CPP solution (ca. 4.14 $g\,l^{-1}$). The symbols represent these experimental profiles. The dotted

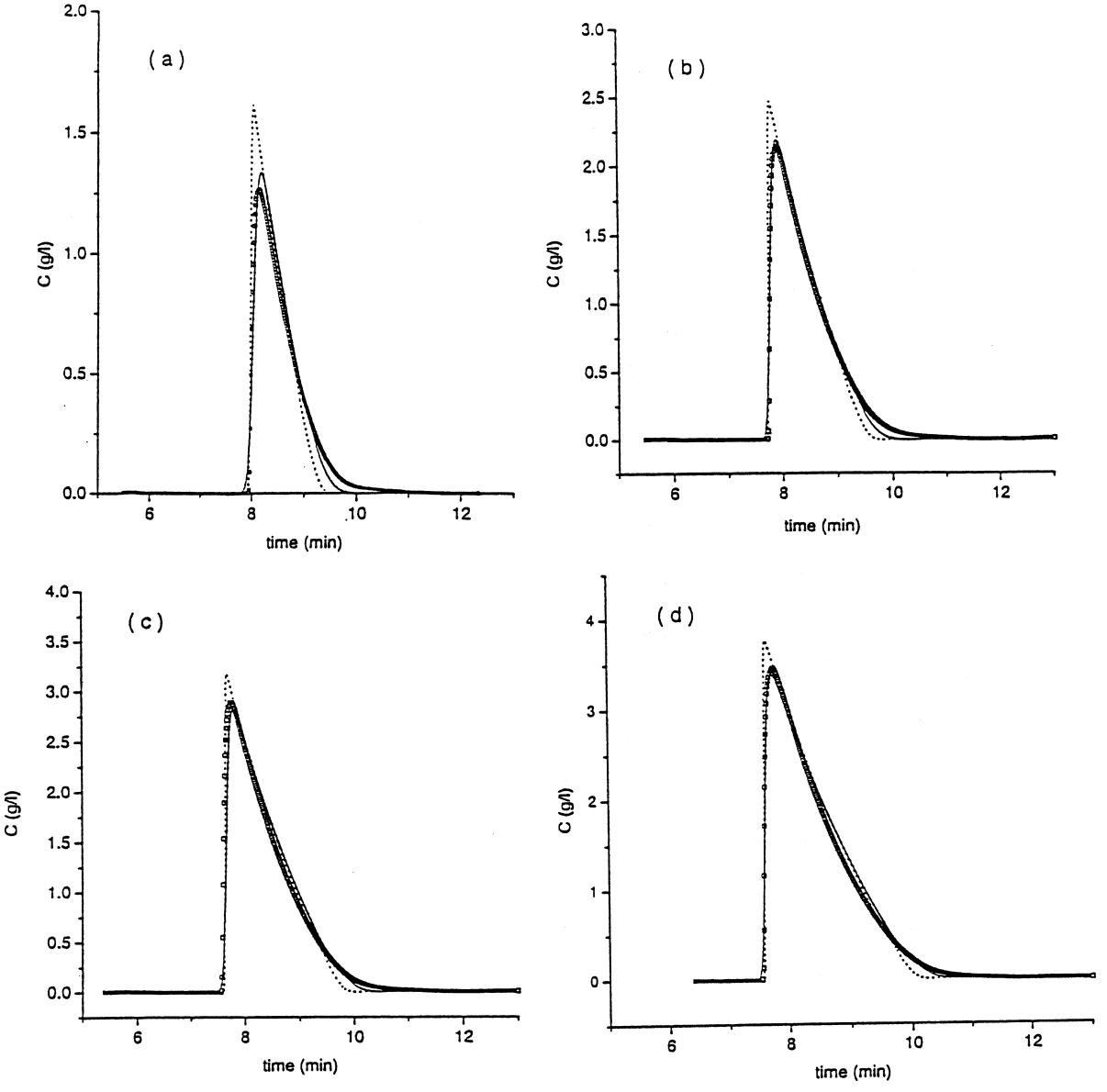

Fig. 4. Experimental and calculated elution profiles for samples of increasing volumes of an *S*-CPP solution ($C = 4.124\ g\,l^{-1}$). Injection volume: (a) 0.25 ml; (b) 0.5 ml; (c) 0.75 ml; and (d) 1.0 ml. Equilibrium-dispersive model (dotted lines) and transport-dispersive model ($k_f = 200\ min^{-1}$) (solid lines).

lines show the band profiles calculated using the equilibrium-dispersive model. The numerical calculations in this case were carried out with an efficiency of 8000 plates, as explained earlier. The solid lines show the best profiles calculated with the transport-dispersive model. The parameters of the Langmuir isotherm determined previously and reported at the bottom of Table 2 were used in all the theoretical calculations.

A good agreement is observed between the calculated profiles based on the equilibrium-dispersive model and the experimental profiles. However, the rear, diffuse boundary of the experimental profiles is always more diffuse than predicted by the model. This can be explained by a mass transfer kinetics slower than included in the model. By contrast, there is an excellent agreement between the experimental profiles and those calculated as numerical solutions of the transport-dispersive model. The different calculated profiles were fitted to the experimental ones by adjusting the value of the rate coefficient, k_f. In these calculations, it was assumed that the axial dispersion coefficient accounted only for half the band variance observed (and measured in the calculation of the efficiency of 8000 plates), the rest arising from the mass resistances. The best value of k_f was found equal to 200 min^{-1} by curve fitting. The same value of the rate coefficient was obtained for the different peak profiles corresponding to increasing sample sizes obtained by increasing the concentration or the injected volumes of the same solution. Finally, note the exact coincidence of the fronts of the experimental and calculated profiles in all cases.

Similar results were obtained for *R*-CPP. The profiles obtained are shown in Fig. 5(a)–(d). The comparison between the experimental profiles (symbols) and the profiles calculated with the equilibrium-dispersive model (dashed lines) or with the transport-dispersive model (solid lines) leads to the same conclusions as in the case of the *S* enantiomer. There is a good agreement between the experimental profiles and those calculated with the equilibrium-dispersive model, especially as far as the fronts of the profiles are concerned. However, the experimental peaks always tail much more than predicted by the model. The agreement between experimental and calculated profiles becomes excellent for the profiles calculated with the transport-dispersive model using a value of the rate coefficient, k_f, equal to 200 min^{-1}. This is the same optimum value as the one determined for the *S* enantiomer.

Fig. 6 compares the experimental elution profiles obtained for an analytical injection of a racemic mixture of *S*- and *R*-CPP (linear chromatography) and the profiles calculated with the two models. Obviously, the best fit was obtained with the transport-dispersive model and 500 min^{-1} for k_f. Careful examination of the figure explains why the column efficiency seems to be high while the peak is tailing and the mass transfer kinetics, although reasonably fast, is slower than expected on a column having such a high efficiency. The peak-width at half-height is the same for the three profiles obtained for each enantiomer, the experimental and the two calculated profiles. But the peak calculated from the equilibrium-dispersive model is Gaussian. The experimental peak and the one calculated with the transport-equilibrium model are not symmetrical but tail slightly because of the finite value of the rate coefficient. Note that profiles calculated with the transport-dispersive model and a rate coefficient $k_f =$ 10 000 min^{-1} were superimposed to those derived from the equilibrium-dispersive model. A decrease of the mass transfer rate coefficient improved the agreement of the calculated profile with the rear diffuse boundary of the experimental profiles for both enantiomers.

There is not a good agreement with the profile calculated with the same model and $k_f = 200$ min^{-1} (Fig. 6). The front of the profile becomes too diffuse. Thus, experimental profiles obtained at low concentrations do not agree with those calculated with the best value of the rate coefficient obtained from high concentration data. This might be explained by a dependence of the mass transfer rate coefficient on the concentration, a phenomenon previously reported [15]. The mass transfer kinetics is certainly more complex than assumed in the transport-dispersive model.

3.3. Binary band profiles

Fig. 7(a)–(d) compare the experimental (symbols) and calculated elution profiles for different sample sizes of the racemic mixtures. All the band profiles

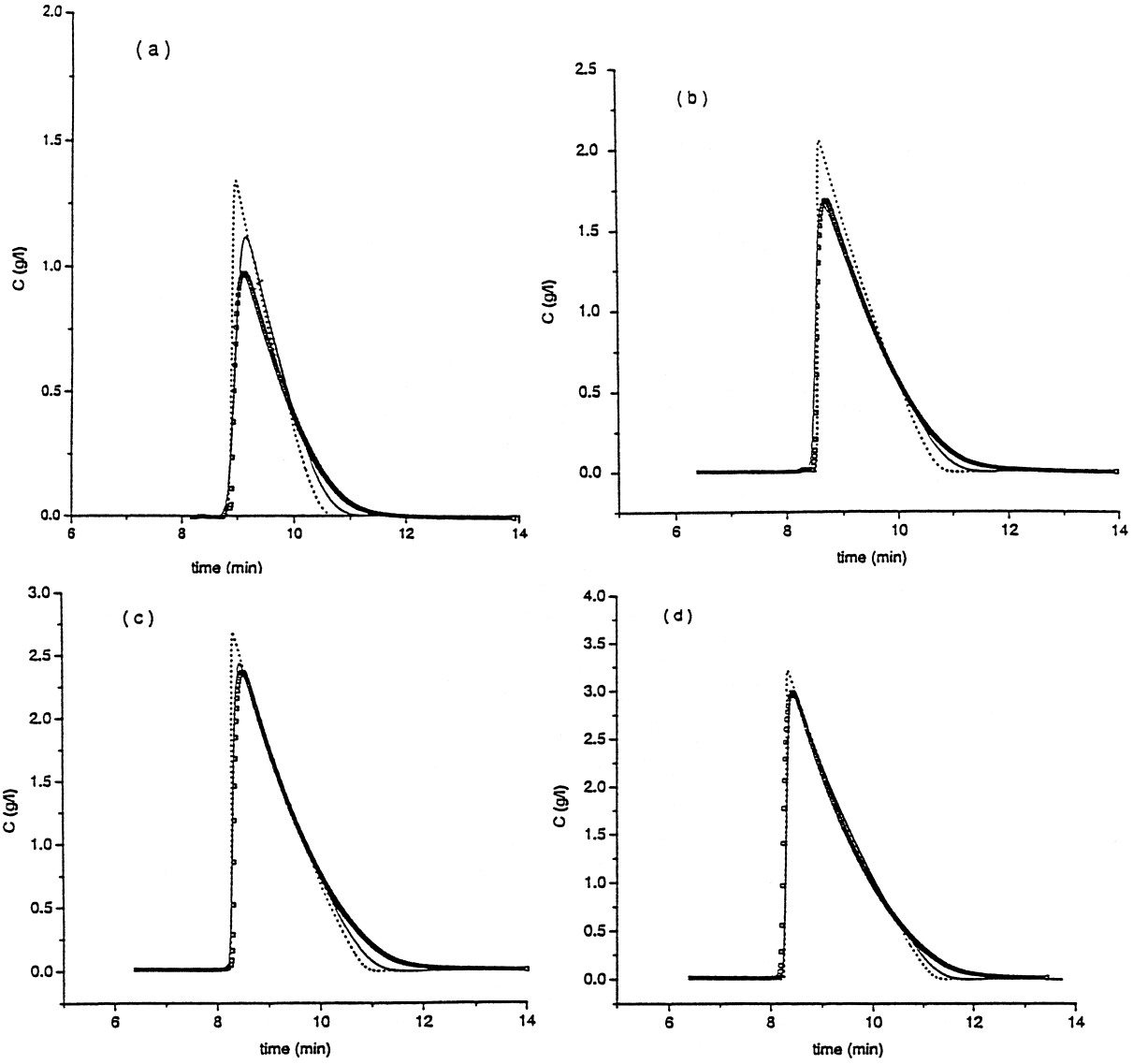

Fig. 5. Experimental and calculated elution profiles for samples of increasing volumes of an *R*-CPP solution ($C = 4.135$ g l^{-1}). Injection volume: (a) 0.25 ml; (b) 0.5 ml; (c) 0.75 ml; and (d) 1.0 ml. Equilibrium-dispersive model (dotted lines) and transport-dispersive model ($k_f = 200$ min^{-1}) (solid lines).

were calculated using the Langmuir competitive isotherm model with the same coefficients as were used to calculate the single-component profiles in Figs. 5 and 6. Again, two sets of profiles were calculated, using the equilibrium-dispersive and the transport-dispersive models. With the former model, the same efficiency was used. With the latter model, we kept the same value of the rate coefficient, at $k_f = 200$ min^{-1}, and of the axial dispersion coefficient. The elution profile based on the latter model agrees well with the experimental data in all four cases. The agreement between the experimental

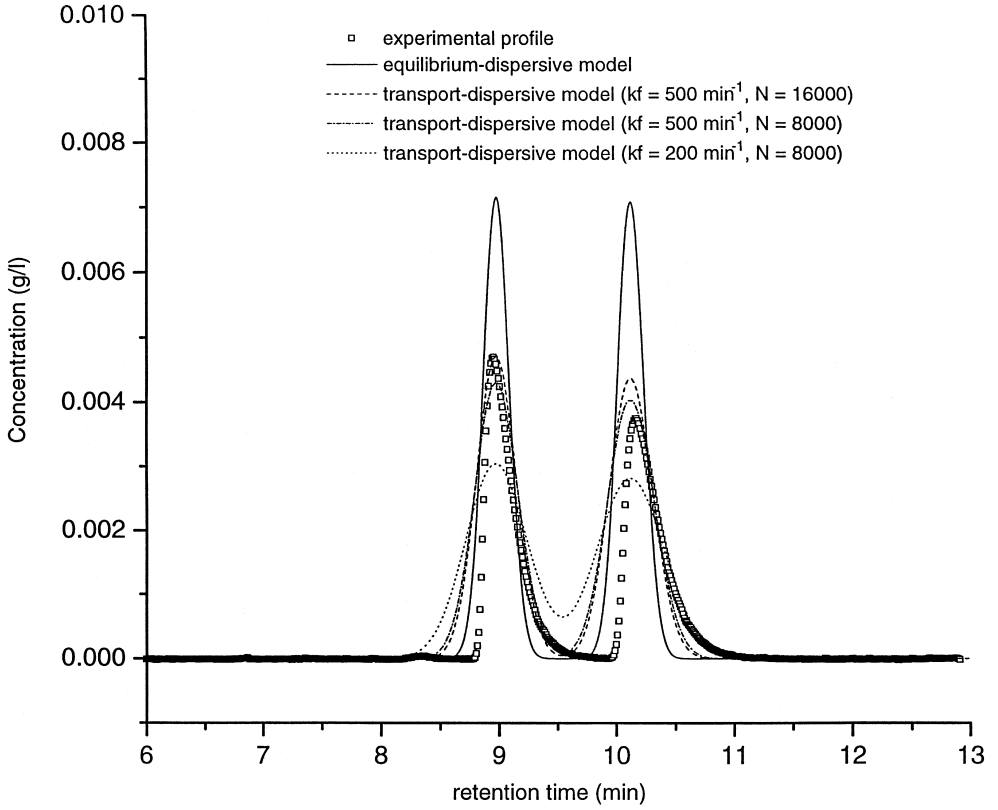

Fig. 6. Experimental and calculated elution profiles under linear conditions for the racemic mixture. Total concentration: 0.2 g l^{-1}; injection volume: 20 μl.

profiles and those calculated with the equilibrium-dispersive model was less satisfactory, especially at high concentrations. The most significant deviations were the tailing of the peaks, unaccounted for, and that the model predicts a worse resolution than the one actually achieved; the valley between the two peaks is always somewhat deeper in the experimental chromatogram than in the calculated one.

4. Conclusion

This study shows that, in certain cases, the simplest isotherm model may account well for the adsorption data obtained in enantiomeric separations. Whereas on chiral stationary phases made of immobilized proteins, the equilibrium isotherm is most generally given by a bi-Langmuir model, the situation appears to be different with cellulose-based phases. Working with cellulose triacetate, Seidel-Morgenstern found for Tröger's base a complex situation, the adsorption isotherm of the less retained enantiomer being given by a Langmuir equation while that of the more retained one was given by a quadratic model [12]. On cellulose trimethylbenzoate, Charton et al. found a bi-Langmuir isotherm for both enantiomers of ketoprofen [13]. On cellulose tribenzoate, we observe a Langmuir isotherm for both enantiomers of 3-chloro-1-phenyl-1-propanol.

However, in the previous two cases the equilibrium-dispersive model accounted well for the band profiles, even though the column efficiency was poor (100 plates on cellulose triacetate [12]) or moderate (1200 plates on cellulose tribenzoate [13]). In this case, the efficiency is much higher and this increase causes a more difficult modeling problem. Simple

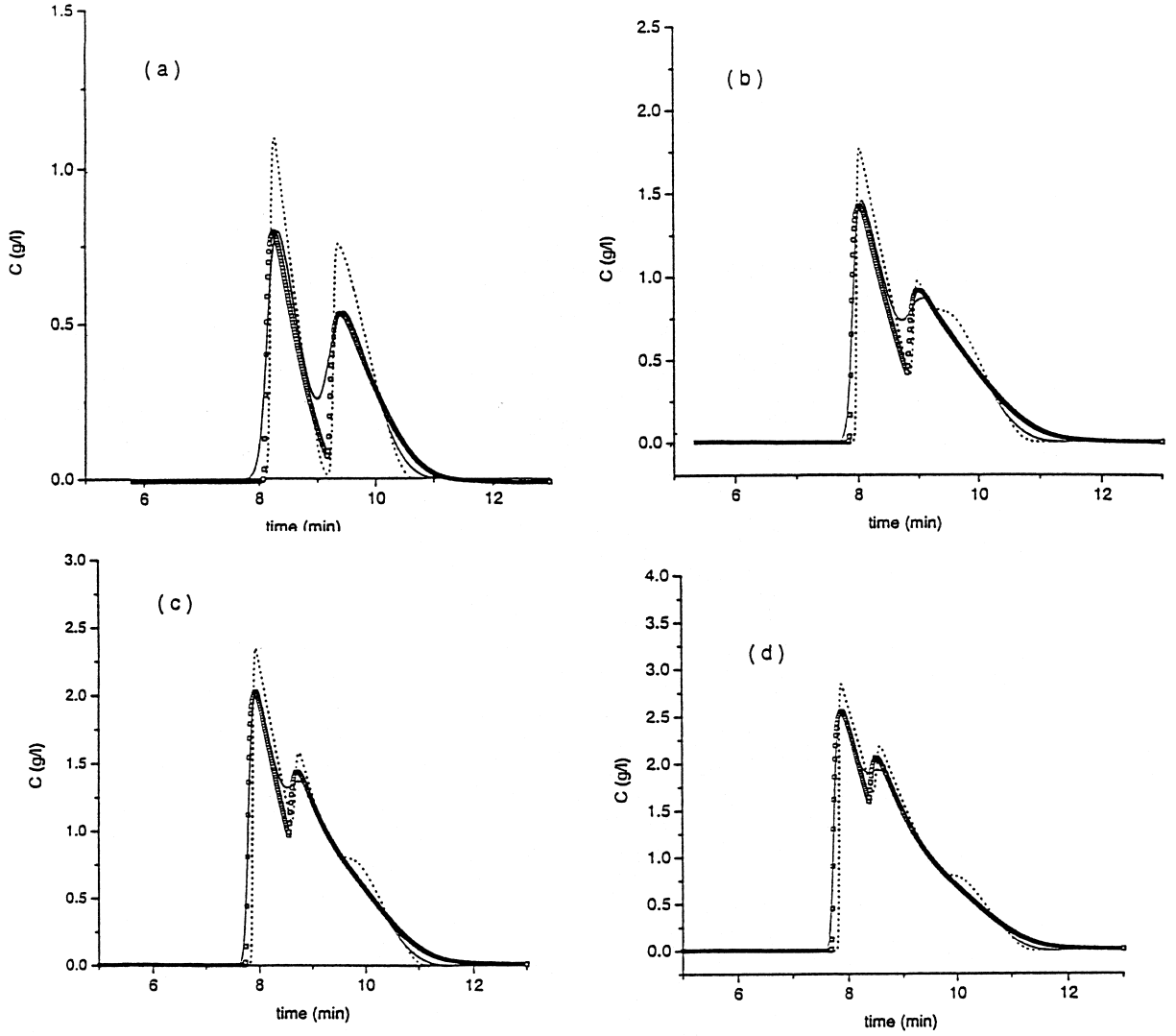

Fig. 7. Experimental (symbols) and calculated elution profiles for sample of increasing volumes of a mixture of *S*-CPP (2.068 g l^{-1}) and *R*-CPP (2.015 g l^{-1}). Injection volume: (a) 0.25 ml; (b) 0.5 ml; (c) 0.75 ml; and (d) 1.0 ml. Equilibrium-dispersive model (dotted lines) and transport-dispersive model (k_f $(S) = k_f(R) = 200$ min^{-1}) (solid lines).

models such as the lumped kinetic model used here are not sophisticated enough.

Acknowledgements

This work was supported in part by Grant No. CHE-97-01680 of the National Science Foundation and by the cooperative agreement between the University of Tennessee and the Oak Ridge National Laboratory.

References

[1] M. Mazzotti, G. Storti, M. Morbidelli, J. Chromatogr. A 769 (1997) 3.
[2] E.R. Francotte, P. Richert, J. Chromatogr. A 769 (1997) 101.

[3] C. Heuer, E. Kusters, T. Plattner, A. Seidel-Morgenstern, J. Chromatogr. A 827 (1998) 175.
[4] L.S. Pais, J.M. Loureiro, A.E. Rodrigues, J. Chromatogr. A 827 (1998) 215.
[5] T. Proll, E. Kusters, J. Chromatogr. A 800 (1998) 135.
[6] C. Migliorini, M. Mazzotti, M. Morbidelli, J. Chromatogr. A 827 (1998) 161.
[7] G. Guiochon, S.G. Shirazi, A.M. Katti, Fundamentals of Preparative and Nonlinear Chromatography, Academic Press, Boston, MA, 1994.
[8] M. Ho Hyun, J. Sung Jin, W. Lee, J. Chromatogr. A 822 (1998) 155.
[9] S.C. Jacobson, S. Golshan-Shirazi, G. Guiochon, J. Am. Chem. Soc. 112 (1990) 6492.
[10] T. Fornstedt, P. Sajonz, G. Guiochon, J. Am. Chem. Soc. 119 (1997) 1254.
[11] T. Fornsted, G. Gotmar, M. Anderson, G. Guiochon, J. Am. Chem. Soc. 121 (1999) 1164.
[12] A. Seidel-Morgenstern, G. Guiochon, Chem. Eng. Sci. 48 (1993) 2787.
[13] F. Charton, S.C. Jacobson, G. Guiochon, J. Chromatogr. A 630 (1993) 21.
[14] T. Fornsted, P. Sajonz, G. Guiochon, Chirality 10 (1998) 375.
[15] P. Sajonz, M. Kele, G. Zhong, B. Sellergren, G. Guiochon, J. Chromatogr. A 810 (1998) 1.
[16] P. Franco, C. Minguillon, L. Oliveros, J. Chromatogr. A 793 (1998) 239.
[17] P. Franco, A. Senso, C. Minguillon, L. Oliveros, J. Chromatogr. A 796 (1998) 265.
[18] R. Landsiedel, H. Frank, H. Glatt, A. Seidel, J. Chromatogr. A 822 (1998) 29.
[19] P. Sajonz, G. Zhong, G. Guiochon, J. Chromatogr. A 731 (1996) 1.
[20] J. Jacobson, J.H. Frenz, Cs. Horvàth, Ind. Eng. Chem. Res. 26 (1987) 43.
[21] P. Sajonz, G. Zhong, G. Guiochon, J. Chromatogr. A 786 (1997) 195.